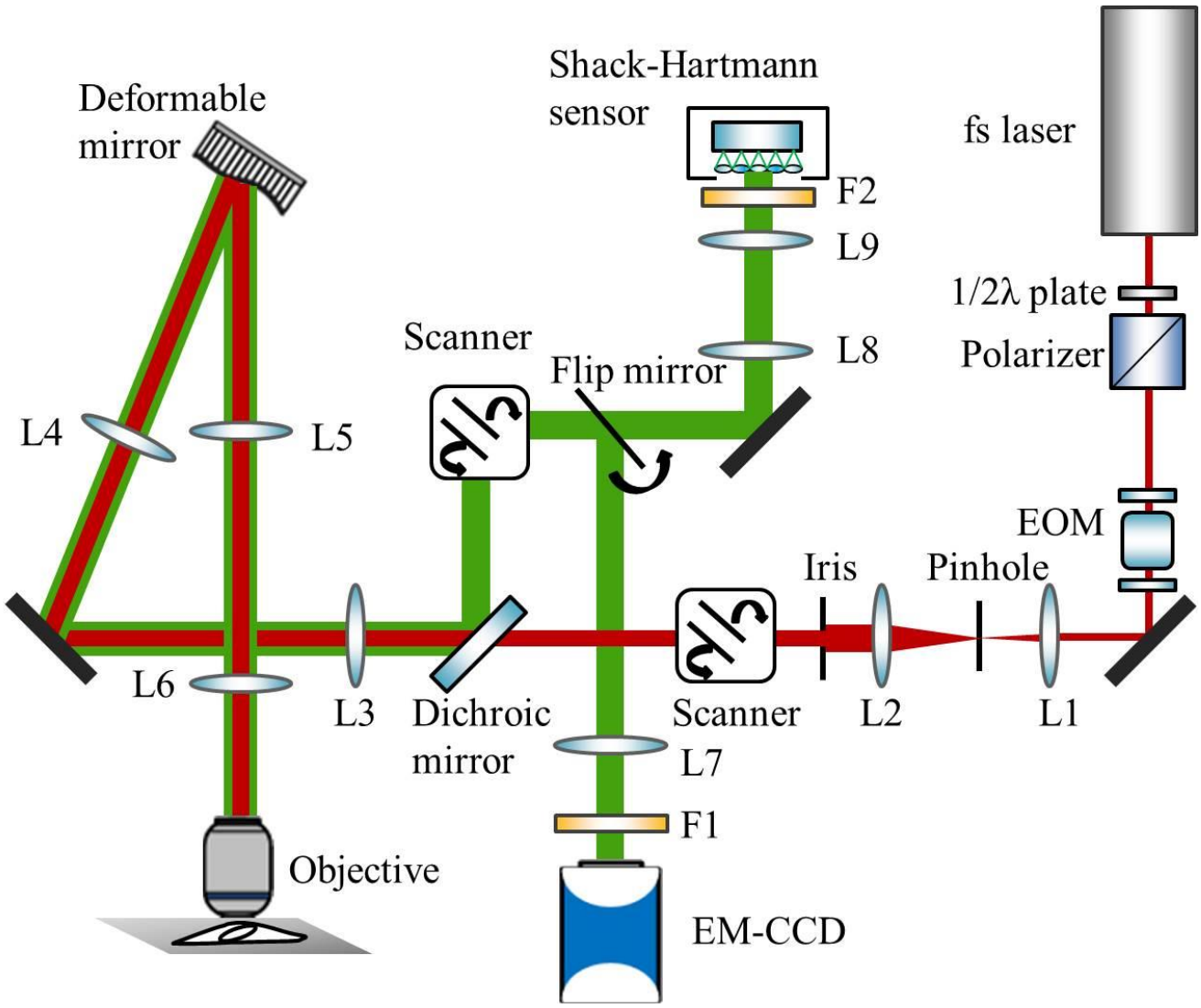

Supplementary Figure 1

Schematic of 2P-ISIM AO optical setup.

Excitation from a femtosecond laser is passed through intensity control and shuttering optics (1/2 λ wave plate, polarizing beam splitting cube, and electro-optic modulator, EOM), spatially filtered (pinhole, 100 μm diameter), beam expanded 5-fold (lens pair L1 and L2, f1 = 40 mm, f2 = 200 mm; and iris) and directed onto a 2D galvanometric mirror (excitation scanner). The point between each galvo surface is made conjugate to a deformable mirror, via lens pair L3 and L4 (f3, f4 = 250 mm). Lens pair L5 and L6 (f5, f6 = 200 mm) images the deformable mirror onto the back focal plane of a 1.2 NA water objective, thereby creating diffraction limited excitation at the sample. Fluorescence is collected along the same path until a dichroic mirror, placed between the excitation scanner and L3, diverts it onto a second 2D galvanometric mirror (emission scanner). Lens pair L4 and L3 images the back focal plane of the objective onto this scanner, which serves to 'rescan' fluorescence emission before imaging onto an electron multiplying CCD (EM-CCD) via lens L7 (f7 = 250 mm), enabling super-resolution imaging. Alternatively, for wavefront measurement, the emission scanner is set to descan the fluorescence, and a flip mirror directs this descanned signal onto a Shack Hartmann sensor. Lens pair L8 and L9 (f8 = 250 mm, f9 = 100 mm) serve to image the point between galvo surfaces in the emission scanner onto the Shack Hartman sensor, thus mapping the back focal plane of the objective onto this sensor. Note that lens pairs L1 and L2; L3 and L4; L5 and L6; and L8 and L9 are placed in 4f imaging configurations, thereby ensuring that the back focal plane of the objective, galvanometric scanners, and deformable mirror are conjugate planes. Filters F1 and F2 serve to reject excitation from reaching the EM-CCD and SHS, respectively. See **Methods, Supplementary Table 2** for more detail.

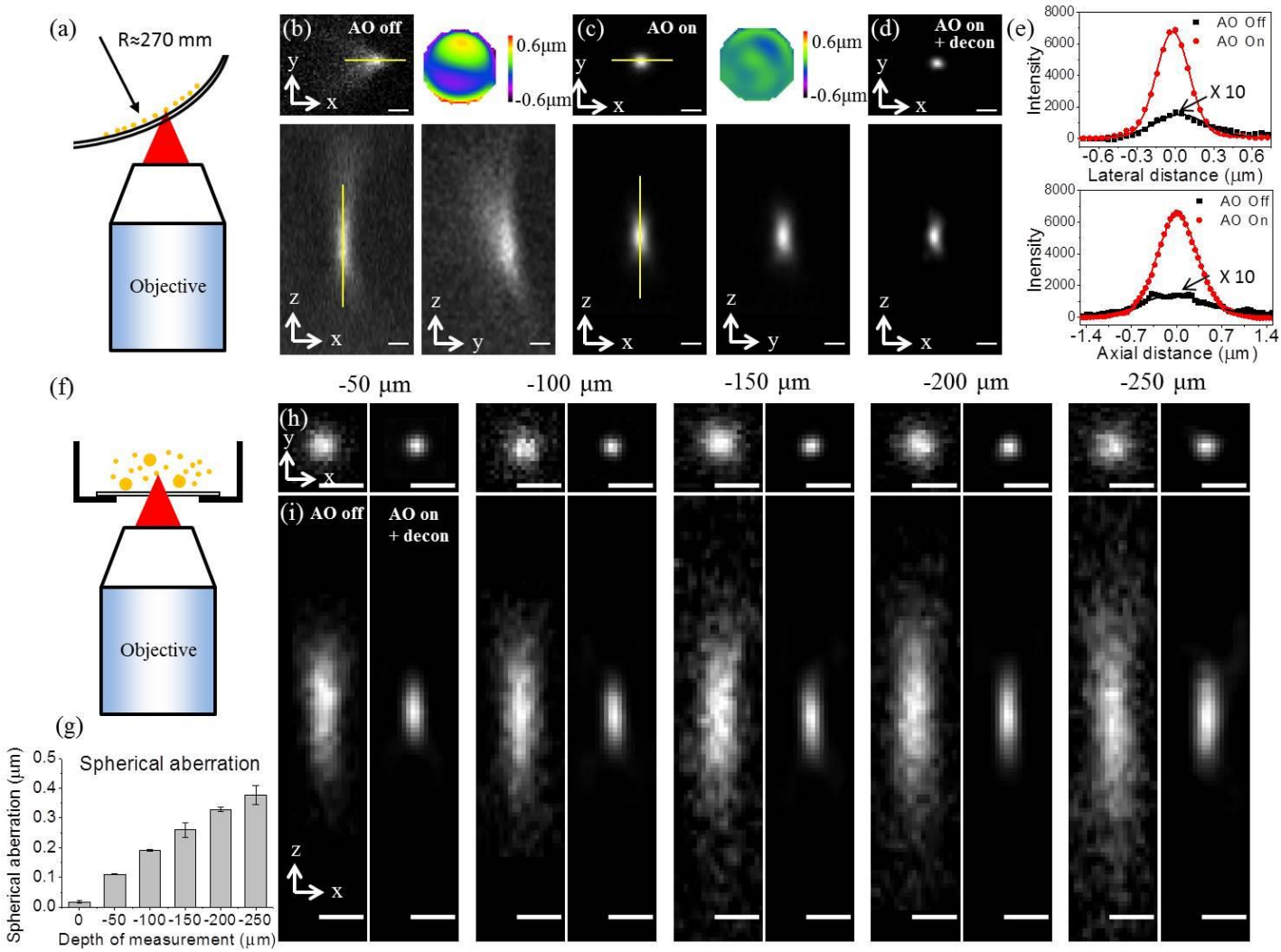

Supplementary Figure 2

AO improves performance of 2P-ISIM in aberrated phantom samples.

a) 200 nm yellow green fluorescent beads were placed within the inner surface of a curved coverslip and imaged without **b)** and with **c)** AO correction, and **d)** subsequently deconvolved. Lateral (top) and axial (bottom) views are shown, as are corresponding wavefront maps (root-mean square, RMS, wavefront error 0.222 µm before AO correction **(c)**, 0.030 µm after AO, **(d)**). **e)** Lateral (top) and axial (bottom) line profiles as indicated in **b-c)** indicate a 40-fold increase in peak signal (note that profiles without AO have been magnified 10-fold for clarity). See also **Supplementary Fig. 4.** For a second test, we embedded 100 nm (small circles) and 1 µm (larger circles) yellow green fluorescent beads within a polyacrylamide gel **f)**. 1 µm beads were used for AO correction due to their strong fluorescence signal, and the nearby 100 nm beads were used for system resolution measurement. Lateral **(h)** and axial **(i)** images through representative beads at indicated depth alternately show images without (odd images) and with (even images) AO correction and subsequent deconvolution. Spherical aberration **(g)** due to the refractive index mismatch increases with depth, and is mitigated using AO at all depths, see also **Supplementary Fig. 5.** Scale bars: 0.5 µm.

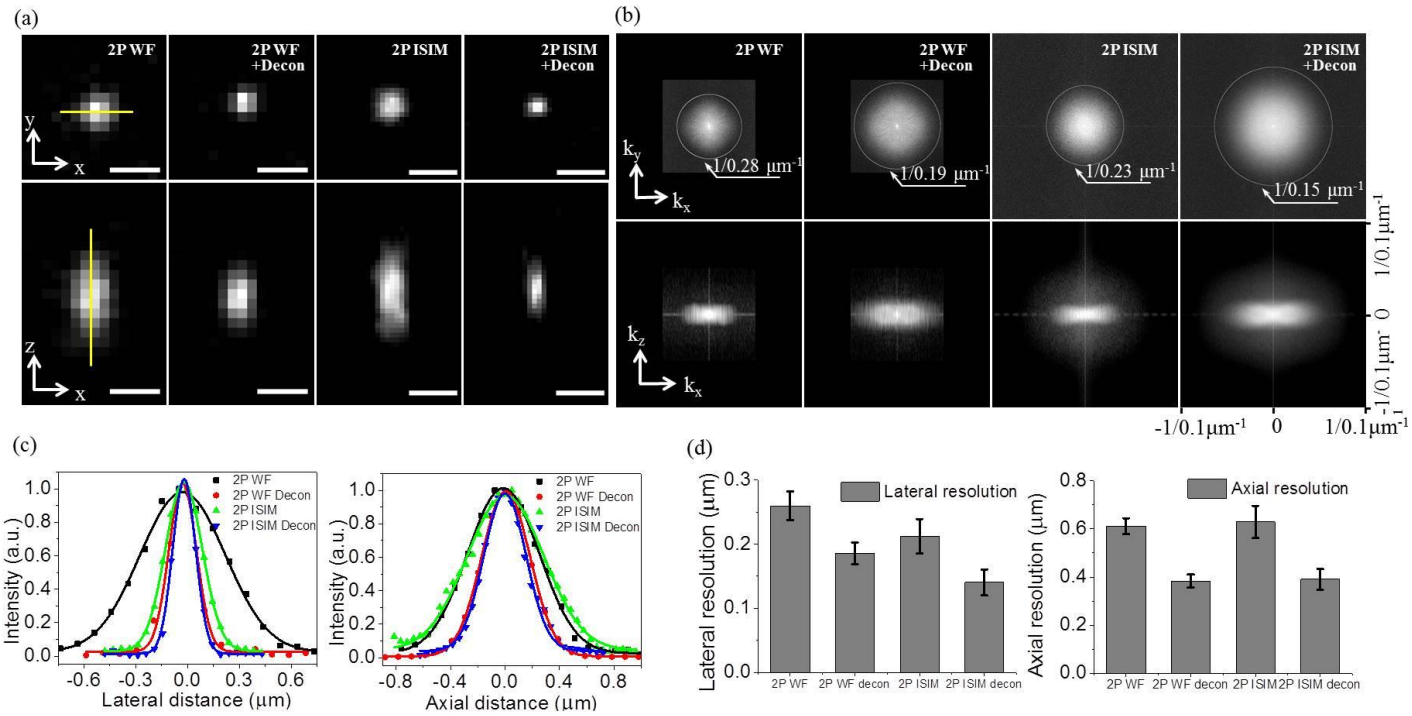

Supplementary Figure 3

Estimating system resolution at coverslip surface in AO-2P ISIM.

a) Exemplary images of 100 nm yellow-green fluorescence beads on coverslip surface, as viewed in lateral (top) and axial (bottom) cuts through the image stacks. From left to right: two-photon wide-field (non-rescan) image, two-photon wide field image after deconvolution, two-photon ISIM image (i.e. after rescanning), two-photon ISIM image after deconvolution. System aberrations were corrected by measuring the wavefront distortion using a Shack-Hartmann sensor, and subsequently compensating for the aberrated wavefront by using a deformable mirror. **b)** Modulation transfer functions corresponding to **a)**. **c)** Comparative line-profiles through the center of each lateral (left) and axial (right) bead image further emphasize improvement after deconvolution. (d) Statistical comparison of estimated lateral (left) and axial (right) resolution (FWHM of bead image), derived from > 30 beads. Means and standard deviations are shown. Scale bars: 0.5 µm.

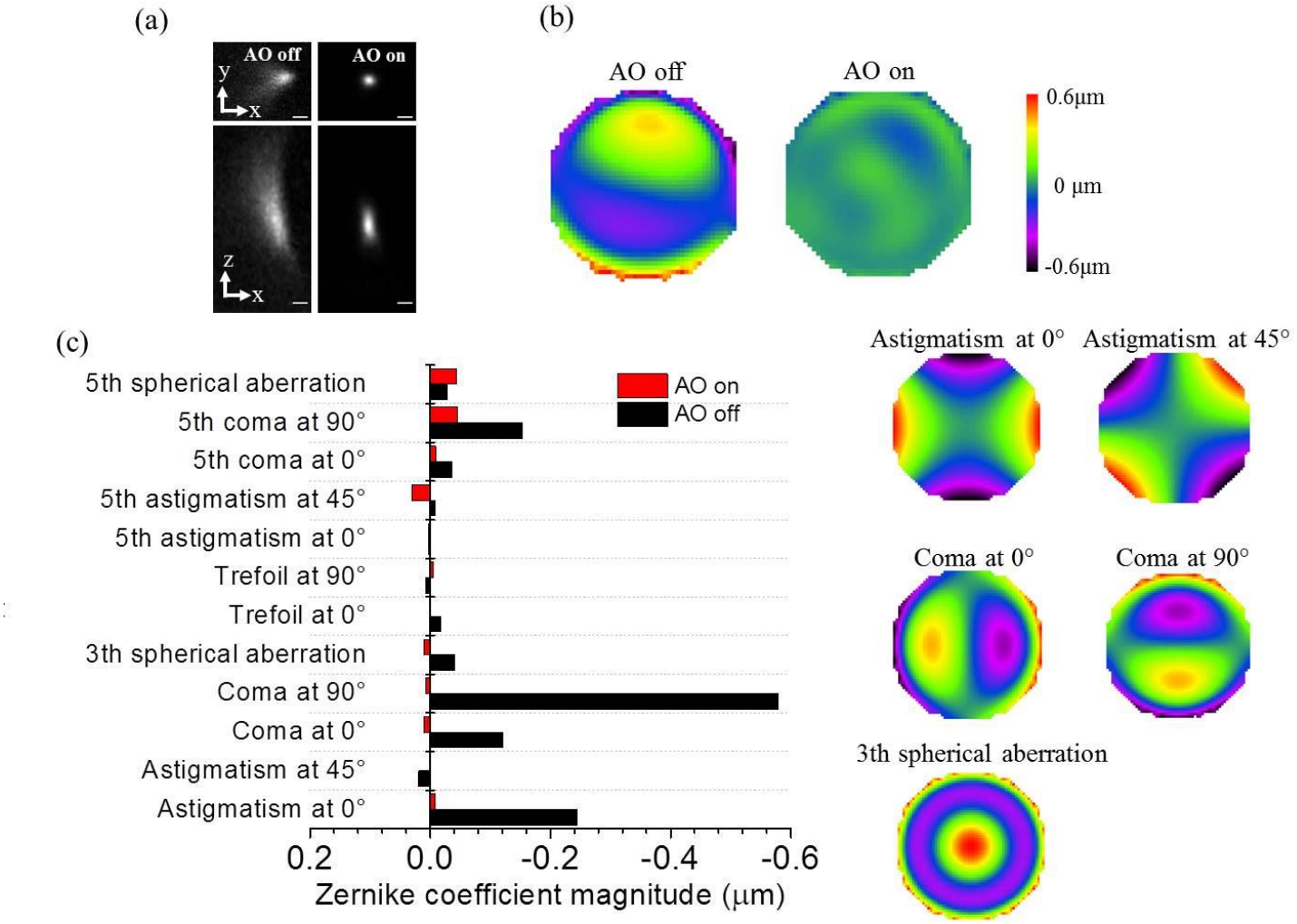

Supplementary Figure 4

Correcting aberrations through a curved glass surface with AO-2P ISIM.

a) Raw (left) and AO-corrected (right) 2P-ISIM images of a 200 nm bead at the curved surface. **b)** Corresponding images of wavefront measured by Shack-Hartmann sensor. RMS wavefront error is 0.222 µm without AO, and 0.030 µm with AO. **c)** Decomposition of wavefront into aberration modes (representative Zernike modes shown at right), indicating substantial astigmatism and coma. See also **Supplementary Fig. 2**. Scale bars: 0.5 µm.

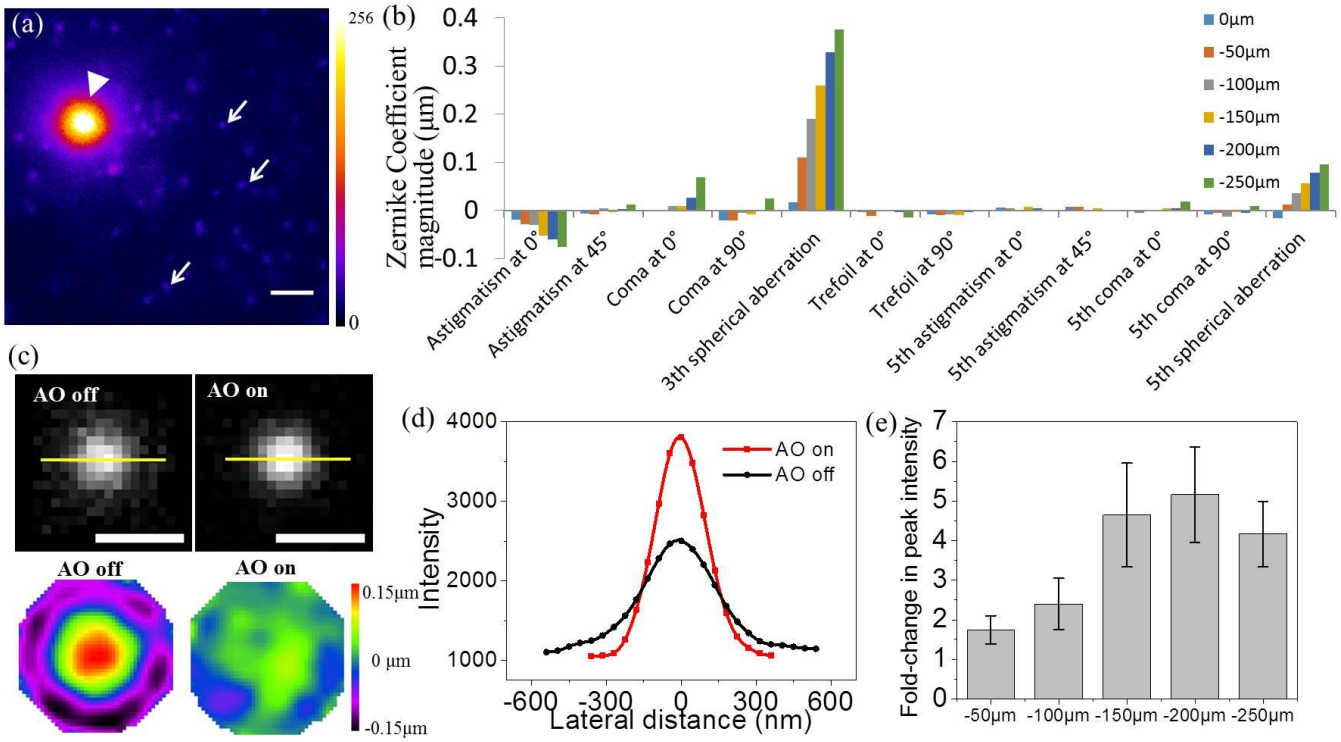

Supplementary Figure 5

Correcting aberrations through a polyacrylamide gel.

a) 2P ISIM fluorescence (pre-AO correction) image measured at depth of 200 µm above the coverslip. The strong fluorescence from 1 µm beads (arrowhead) was used for AO correction and the nearby 100 nm beads (arrows) were used for resolution assessment. **b)** Decomposition of wavefront into Zernike aberration modes, indicating substantial spherical aberration due to refractive index mismatch. Aberration modes are color-coded according to depth in polyacrylamide gel. **c)** Representative lateral slices (top) and corresponding wavefront maps (bottom) through 100 nm yellow green beads 50 µm into gel, indicating apparent size of bead without (left) and with (right) correction. No deconvolution was applied. **d)** Intensity line profiles as indicated in **c)**. Note ~2x increase in peak intensity. **e)** Statistical comparison of relative peak intensity increase after AO correction at indicated depth in the sample. Data are derived from 10 beads. Means and standard deviations are shown. See also **Fig. 2**. Scale bars: 2 µm in **a)**, 0.5 µm in **c)**.

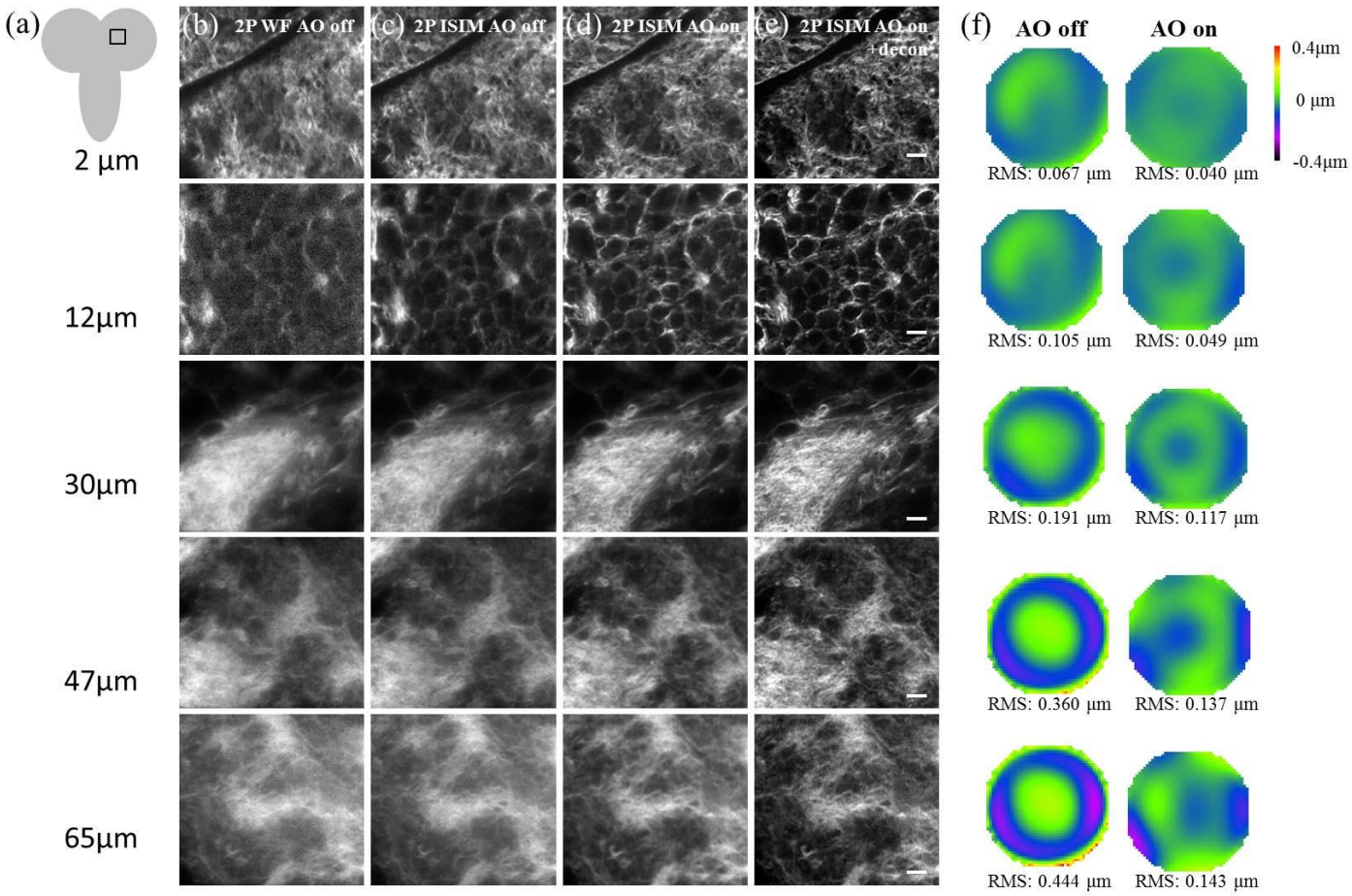

Supplementary Figure 6

AO improves 2P ISIM imaging at depth in *Drosophila* tissue.

a) Schematic of brain lobe, square indicates imaging region. Comparative images at indicated depth (rows), showing 2P excitation, no rescan (**b**); raw 2P ISIM (**c**); raw 2P ISIM with AO correction (**d**); 2P ISIM deconvolved after AO correction (**e**). **(f)** Wavefronts are shown before (left column) and after (right column) aberration correction; root mean square (RMS) values are also indicated. See also **Fig. 1, Supplementary Video 1**. Scale bars: 5 µm.

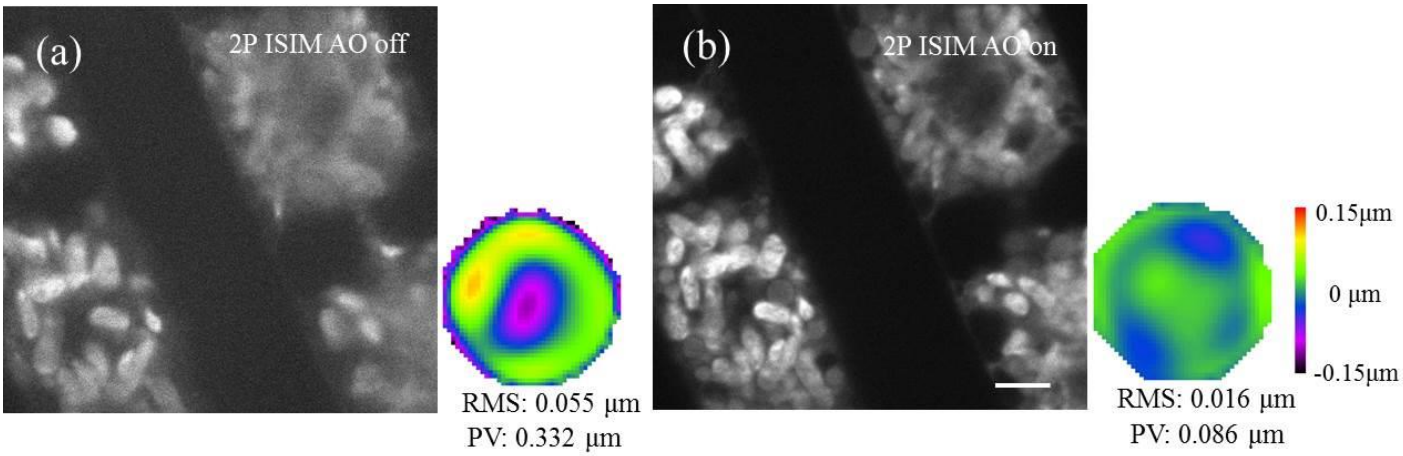

Supplementary Figure 7

2P ISIM images of Zygnema algae.

Before (**a**) and after (**b**) wavefront correction. Autofluorescence from the sample was used to derive wavefronts in each case, which are shown to the right of each image (RMS and peak-to-valley values are also shown). Images were acquired 7 µm into the stack (the largest algal cross-section in our imaging field) and ~50 µm from the coverslip. Scale bar: 5 µm.

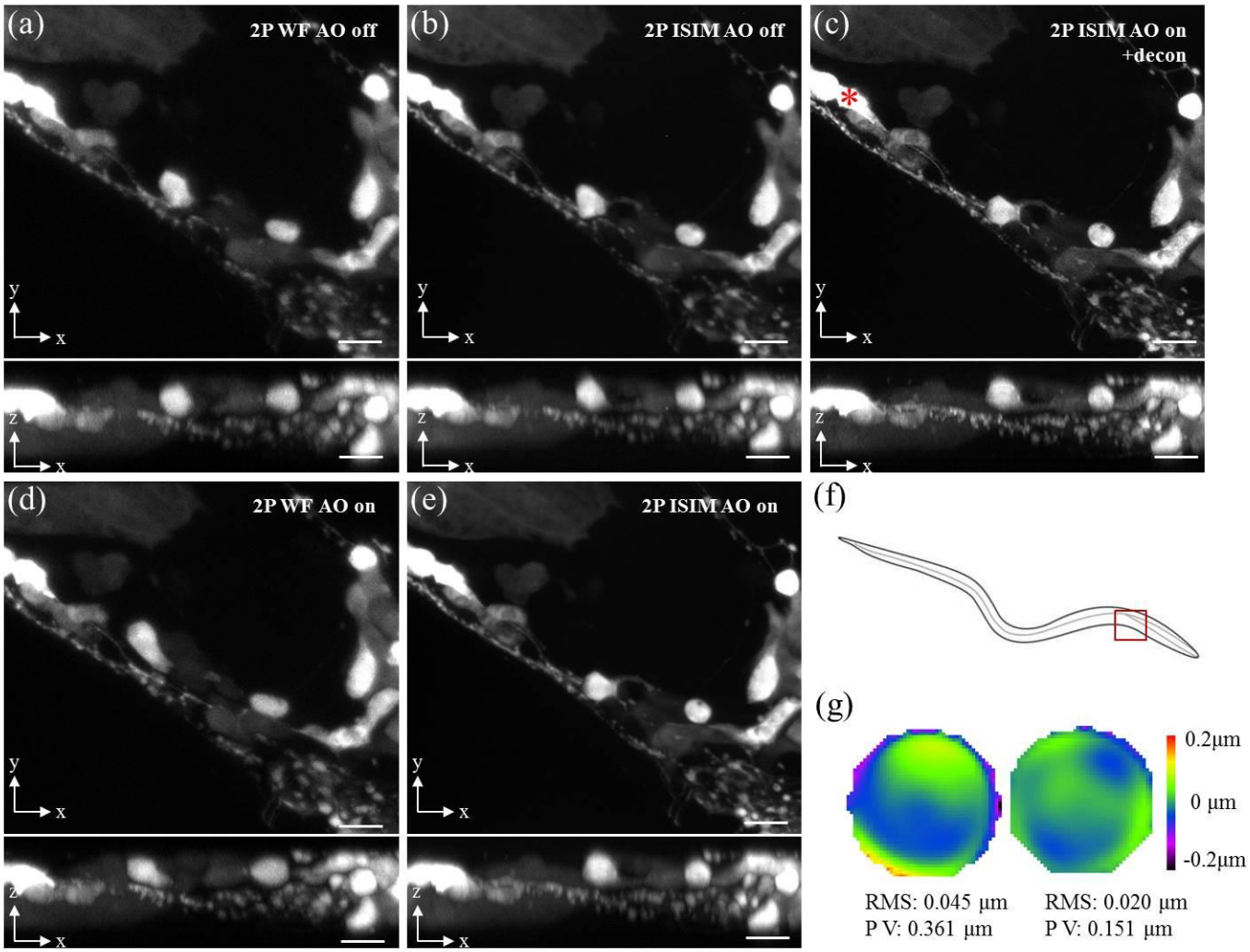

Supplementary Figure 8

Fiducial-based AO Correction in live biological samples, as demonstrated in larval nematodes expressing GFP.

Neural structures were tagged with GFP in larval nematodes and imaged without rescan (**a,** no AO; **d**, with AO), with rescan (**b**, without AO; **e**, with AO) and with rescan and followed by deconvolution **(c)**. The best resolution and contrast are obtained in **(c)**. Lateral (upper) and axial maximum intensity projections are shown. The field of view was chosen near the head of the animal as indicated by red box in schematic **f)**. Comparative wavefronts before and after AO correction are shown in (**g**); wavefronts were derived by scanning the beam over the neuron marked with red asterisk in **(c)**. In this sample, the cell body region marked in **(c)** was used for AO. Scale bars: 5 µm.

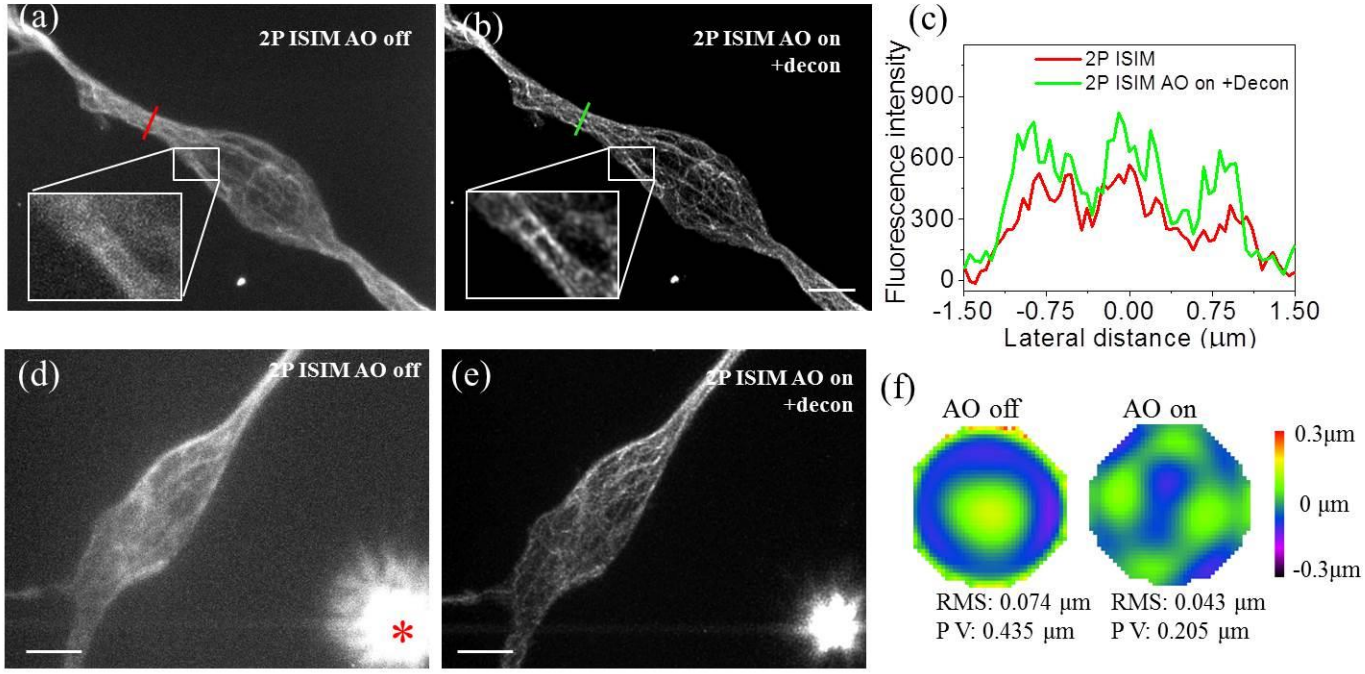

Supplementary Figure 9

Fiducial-based AO correction improves 2P ISIM imaging of microtubule bundles in fixed cells embedded in a 3D matrix, at depths exceeding 200 µm from the coverslip surface.

Results without **(a, d)** and with **(b, e)** AO correction and subsequent deconvolution. The latter images show obvious improvements in spatial resolution and contrast (compare insets in **a, b**) and signal (line profiles in **c**, corresponding to red/green lines indicated in **a**, **b**. Representative images are shown 50 µm (**a, b**) and 230 µm (**d, e**) from the coverslip. From the MTFs (see **Methods** for details on calculations), we estimate that AO improves the lateral resolution from 0.45 µm (**a**) to 0.20 µm (**b**) and the axial resolution from 1.50 µm (**a**) to 0.55 µm (**b**) 50 µm from the coverslip. AO improved lateral resolution from 1.05 µm (**d**) to 0.33 µm (**e**) and axial resolution from 2.34 µm (**d**) to 0.65 µm (**e**) 230 µm from the coverslip. Images (**d, e**) also show the fluorescent bead (red asterisk in **d**) used for correction; note that image contrast has been adjusted to show the much fainter signal in the biological sample, which is why bead appears saturated. Comparative wavefronts corresponding to (**d, e**) are shown in (**f**)**.** All images are maximum intensity projections. Scale bars: 5 µm.

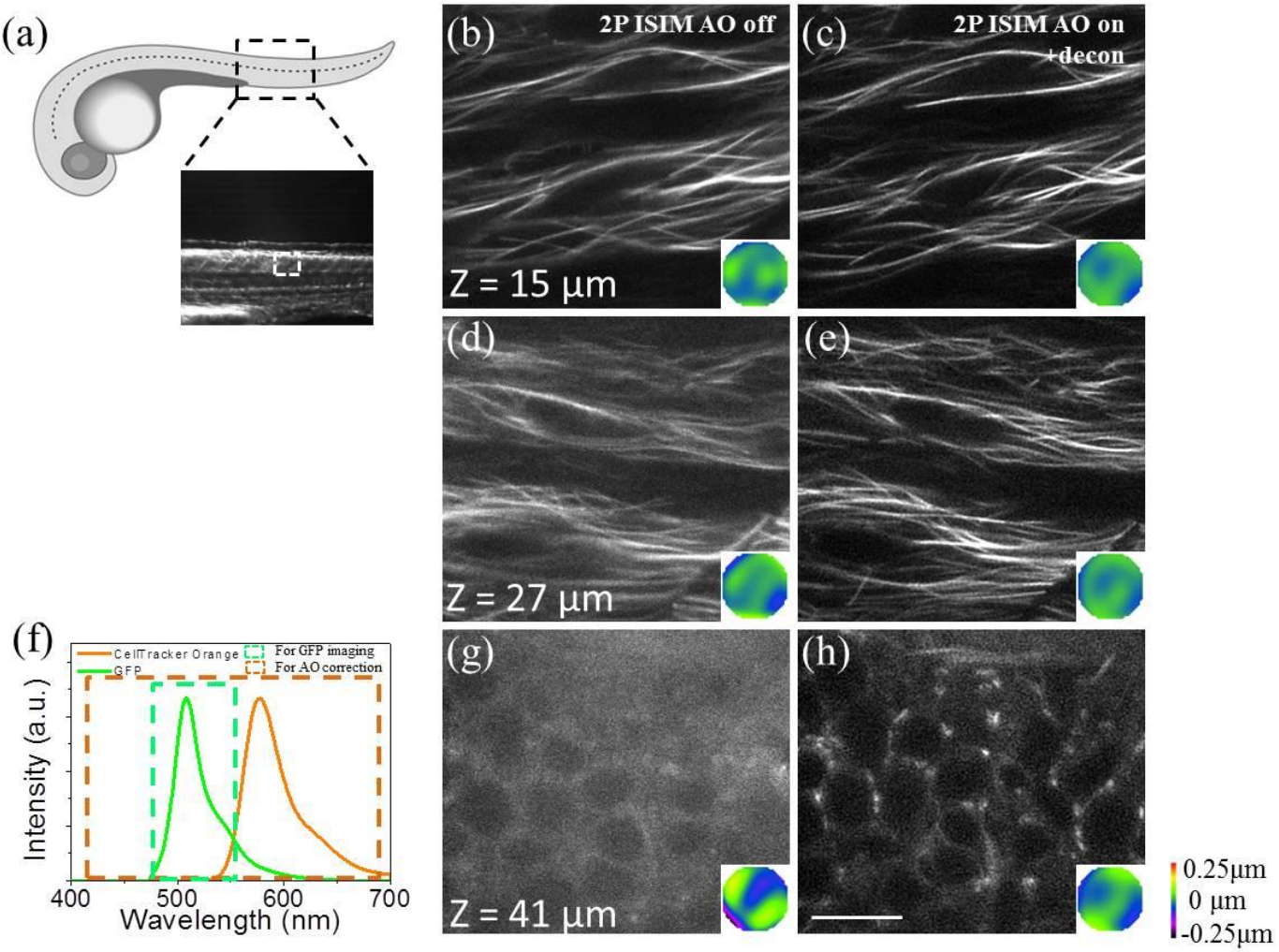

Supplementary Figure 10

Dye-based AO improves 2P-ISIM imaging in somites (b-e) and neural tube (g-h) of live embryonic zebrafish at 30-32 hpf.

a) Schematic of embryo, indicating imaging region (higher magnification view). Selected imaging fields at indicated axial depth are shown, before **(b, d, g)** and after **(c, e, h)** AO correction and subsequent deconvolution. Comparative wavefronts are also shown as inset. **f)** Indicates spectral bandwidth used for AO correction with CellTracker Orange and 2P-ISIM imaging. See also **Fig. 3**. Scale bar: 10 µm.

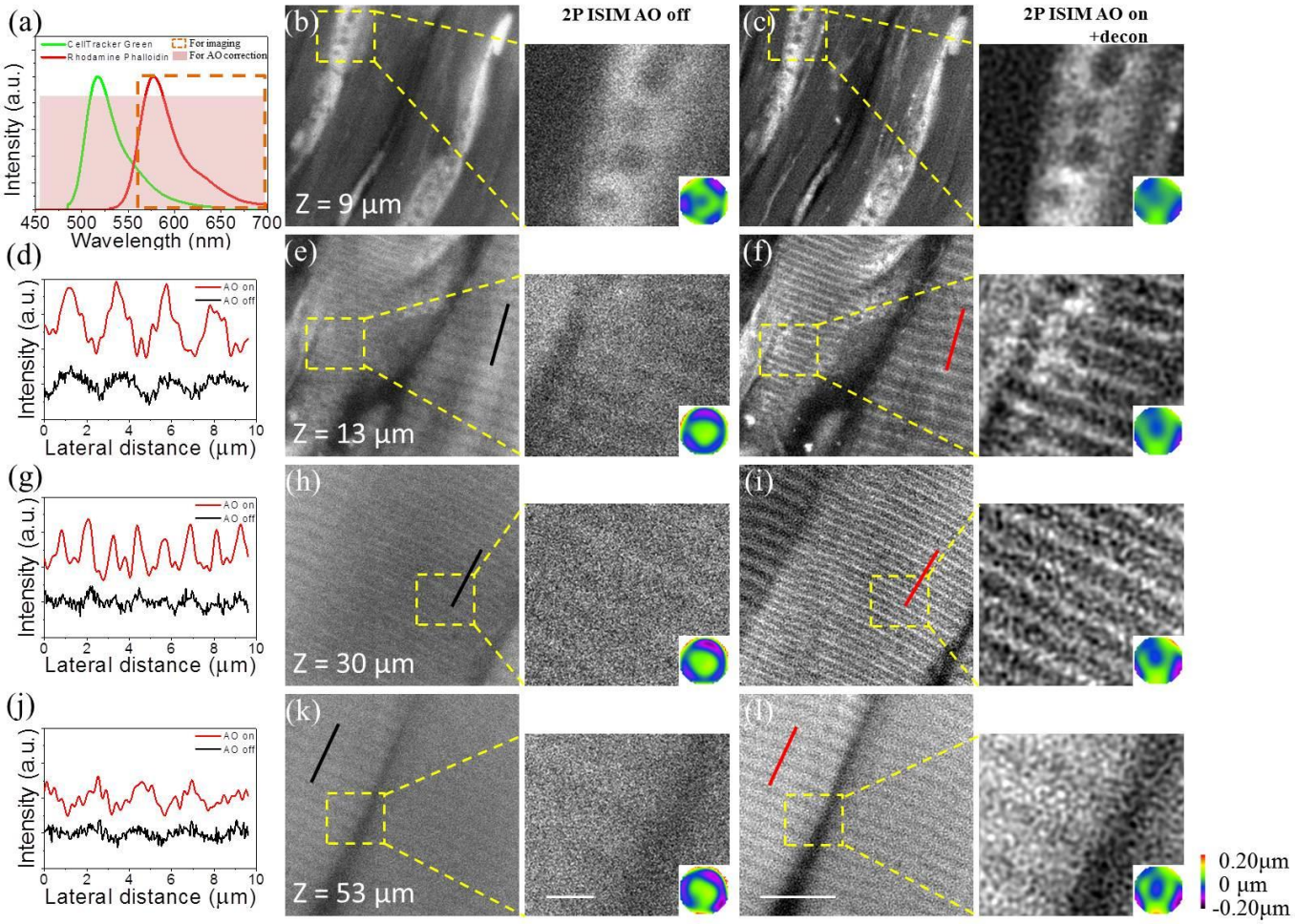

Supplementary Figure 11

Dye-based AO improves 2P-ISIM imaging of gastrocnemius muscle of excised mouse leg.

Rhodamine phalloidin was used to stain actin fibers within the muscle leg and CellTracker Green was added for AO correction. **a)** Graph indicates spectral region used for AO correction vs. imaging. Selected image slices through two gastrocnemius muscle fibers of differing contractility before (**b, e, h, k**) and after **(c, f, i, l)** AO and deconvolution. Normalized line profiles (40 pixels in width) corresponding to red/black lines indicated in each depth are shown in (**d, g, j**). Higher magnification views of dashed yellow rectangular regions are shown, as are wavefronts (insets). Scale bars: 5 µm for zoomed-out panels, 2 µm for higher magnification views.

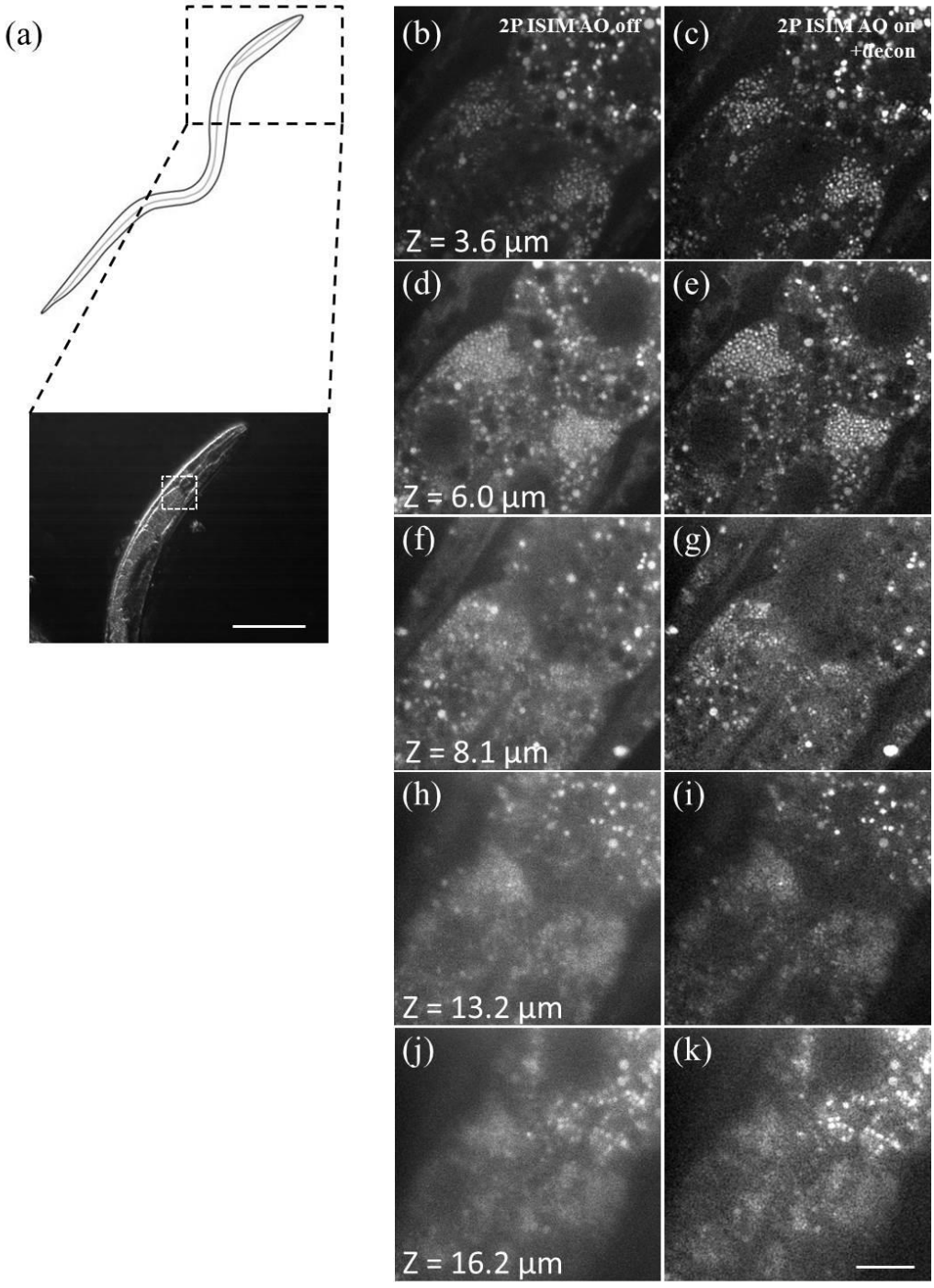

Supplementary Figure 12

Dye-based AO improves 2P-ISIM imaging of presumed gut granules in live larval *C. elegans*.

a) Schematic of larvae, indicating approximate region (higher magnification views) used in imaging. Worms were incubated overnight with CellTracker Orange mixed with OP50 prior to imaging. The 400 nm-700 nm spectral region was used for AO correction. Imaging was performed before **(b, d, f, h, j**) and after **(c, e, g, i, k**, all with subsequent deconvolution) AO, using a 525/70 bandpass emission filter. Scale bar in brightfield transmission image: 100 µm; in fluorescence images: 10 µm.

Supplementary Table 1, Adaptive recovery of resolution at progressively increasing distances from the coverslip (aberrations increase with distance).

	Lateral system resolution (0 μm, at coverslip)	**-50 μm**	**-100 μm**	**-150 μm**	**-200 μm**	**-250 μm**
2P WF AO off		300 ± 23 nm		328 ± 24 nm		350 ± 33 nm
2P WF AO on	260±22 nm	267 ± 11 nm		287 ± 25 nm		313 ± 27 nm
2P WF AO on + decon	186±17 nm	161 ± 9 nm		183 ± 18 nm		219 ± 19 nm
2P ISIM AO off		249 ± 19 nm	270 ± 11 nm	272 ± 35 nm	290 ± 13 nm	302 ± 26 nm
2P ISIM AO on	212 ± 27 nm	228 ± 7 nm	229 ± 7 nm	229 ± 9 nm	238 ± 11 nm	259 ± 17 nm
2P ISIM AO on + decon	140 ± 20 nm	142 ± 7 nm	142 ± 5 nm	146 ± 7 nm	151 ± 8 nm	176 ± 10 nm
	Axial system resolution (0 μm, at coverslip	**-50 μm**	**-100 μm**	**-150 μm**	**-200 μm**	**-250 μm**
2P WF AO off		1047 ± 82 nm		1351 ± 99 nm		1686 ± 163 nm
2P WF AO on	611±32 nm	684 ± 34 nm		799 ± 36 nm		1029 ± 49 nm
2P WF AO on + decon	383±27 nm	389 ± 16 nm		497 ± 42 nm		664 ± 35 nm
2P ISIM AO off		966 ± 81 nm	1120 ± 37 nm	1274 ± 63 nm	1397 ± 83 nm	1616 ± 112 nm
2P ISIM AO on	629±67 nm	695 ± 15 nm	788 ± 41 nm	887 ± 42 nm	943 ± 40 nm	1032 ± 45 nm
2P ISIM AO on + decon	390±43 nm	439 ± 16 nm	513 ± 30 nm	594 ± 27 nm	623 ± 33 nm	729 ± 39 nm

100 nm fluorescent beads were placed in a polyacrylamide gel and imaged as indicated (left column) at indicated depth. In all cases, AO correction (using nonlinear-excitation induced signal derived from 1 μm fluorescent beads) improved lateral and axial resolution, as indicated by FWHM values measured from 100 nm beads. At least 10 beads were used for measurements.

Nature Methods: doi:10.1038/nmeth.4337

Supplementary Table 2, Acquisition parameters and fluorescence filters used in this work.

Sample	Figure/Video	Excitation Wavelength, nm	2P-ISIM Imaging, F1	Wavefront Sensing, F2	Frame Acquisition, s	Frame Average	Axial Step, nm	Number of planes	Volume Imaging Time , s
Beads	S2a,S3,S4	900	FF01-720/SP	FF01-720/SP	0.5	10	100	45	240
	S2b,S5	900	FF01-720/SP	FF01-720/SP	0.5	10	100	40	210
Cells in gel	2, Video 3	830	FF01-720/SP	FF01-720/SP	0.5	5	300	50	140
	S9	930	FF01-720/SP	FF01-720/SP	0.5	5	300	50	140
Zygnema algae	S7	900	FF01-720/SP	FF01-720/SP	0.5	5	500	15	60
Drosophila larval brain	1, S6, Video 1	930	FF01-520/70-25	FF01-720/SP	0.5	5	500	150	700
Zebrafish embryos	3, S10, Video 4	900	FF01-520/70-25	FF01-720/SP	0.5	5	1000	70	280
Nematode embryos	Video 2	930	FF01-720/SP & FF01-520/70	FF01-720/SP	0.5	1	1000	30	20
Larval nematodes	S8	900	FF01-720/SP	FF01-720/SP	0.5	5	300	40	110
	S12	850	FF01-720/SP & FF01-520/70-25	FF01-720/SP	0.5	5	300	65	260
Mouse leg	S11	870	FF01-720/SP & FF562-Di03-25x36	FF01-720/SP	0.5	5	1000	60	240

Frame Average: the number of raw frames averaged to produce a single image; Axial Step: the axial step size between planes; Number of planes: the total number of planes in a 3D volume; Volume Imaging Time: total time for acquiring a 3D volume, including imaging, frame averaging, wavefront measurement, and instrument overhead (~0.5 s, including flipping mirror, moving piezoelectric stage). All fluorescence filters are from Semrock; F1 and F2 refer to **Supplementary Fig. 1**.

Nature Methods: doi:10.1038/nmeth.4337